

Article

Thermal Maturity of the Grajcarek Unit (Pieniny Klippen Belt): Insights for the Burial History of a Major Tectonic Boundary of the Western Carpathians

Magdalena Zielińska 

Faculty of Natural Sciences, Institute of Earth Sciences, University of Silesia in Katowice, 60 Bedzinska St., 41-200 Sosnowiec, Poland; magdalena.zielinska@us.edu.pl

Abstract: The Grajcarek Unit of the Pieniny Klippen Belt (PKB), at the boundary between the Central (Inner) and Outer Carpathians, resulted from the convergence of the ALCAPA (the Alps–Carpathians–Pannonia) block and European plate. The strongly deformed slices of the Grajcarek Unit consist of Jurassic–Cretaceous sedimentary rocks associated with Late Cretaceous–Middle Palaeocene synorogenic wild-flysch, and sedimentary breccias with olistoliths. Maximum burial temperatures and burial depths were estimated based on vitrinite reflectance data. The vitrinite reflectance values were wide scattered through the Grajcarek sedimentary succession, especially in the flysch formations. This is attributed mainly to the depositional effects that affected the vitrinite evolution. The determined maximum burial temperatures were interpreted due to the regional compression controlled by tectonic burial coeval with thrusting and strike-slip faulting. The regional vitrinite reflectance variations might estimate cumulative displacement around the NNW–SSE and oriented the strike-slip Dunajec fault, which is a continuation of the deep fracture Kraków–Myszków fault zone.

Keywords: Western Carpathians; Pieniny Klippen Belt; vitrinite reflectance; thermal maturity; burial depth; organic matter



Citation: Zielińska, M. Thermal Maturity of the Grajcarek Unit (Pieniny Klippen Belt): Insights for the Burial History of a Major Tectonic Boundary of the Western Carpathians. *Minerals* **2021**, *11*, 1245. <https://doi.org/10.3390/min11111245>

Academic Editor:
Manuel Francisco Pereira

Received: 28 July 2021
Accepted: 7 November 2021
Published: 10 November 2021

Publisher's Note: MDPI stays neutral with regard to jurisdictional claims in published maps and institutional affiliations.



Copyright: © 2021 by the author. Licensee MDPI, Basel, Switzerland. This article is an open access article distributed under the terms and conditions of the Creative Commons Attribution (CC BY) license (<https://creativecommons.org/licenses/by/4.0/>).

1. Introduction

The useful phenomena of vitrinite reflectance (VR) as the main parameter for maturity determination can be attributed to several reasons: (a) vitrinite or vitrinite-like macerals are present in almost organic-rich sedimentary or metasedimentary rocks; (b) vitrinite exhibits a wide temporal and spatial distribution; (c) VR measurements are relatively quick and simple to obtain. The increase in VR is primarily caused by temperature increase being an irreversible process, thus recording maximum thermal stress [1]. Vitrinite reflectance is commonly used to identify and analyse various geological phenomena (faulting, thrusting, uplift and erosion, intrusion) to decipher thermal history in sedimentary basins [2–14]. These aspects are relevant in fold and thrust belts characterised by the juxtaposition of rocks with a different thermal peak where both strike-slip and extensional tectonics can rework the thrust stack during the later stages of deformation. In such cases, organic parameters of the thermal evolution of sedimentary rocks are often used to obtain a tectonic loading produced by orogeny [15–18].

This research aimed to obtain data on the regional thermal maturity of the Grajcarek Unit. It quantified the maximum burial depths resulting from the shortening and general northward thrusting of the Pieniny Klippen Belt due to the collision between the European Platform and Alps–Carpathians–Pannonia (ALCAPA) units belonging to the Adriatic paleogeographic domain (e.g., [19,20]). Defining the thermal history of the Grajcarek Unit is, therefore, crucial for a better understanding of the tectonic evolution of the whole Carpathian orogenic belt and identification of targets in hydrocarbon exploration and production. Moreover, the analytical results can be further used as comparative data for

geochemical and sedimentological studies of source areas and/or burial history including thermochronometry or paleobathymetry of the fold and thrust belts.

Geological Setting

The Central Western Carpathian–North European suture zone follows the Pieniny Klippen Belt (PKB), a distinctive tectonic zone stretching from Slovakia through Poland up to Romania (Figure 1a). PKB in the West Carpathians is a particular narrow orocline segment that contains Mesozoic to Cenozoic blocks (klippen) surrounded by flysch, shaly, and marly matrix (e.g., [21–31]). The PKB was formed during deformation in a backstop position between the Outer Carpathian accretionary wedge and the bulldozing Central Carpathians thick-skinned thrust stack [32–38]. The klippen structure is interpreted as the olistoliths and olistostromes derived from the Central Carpathian Mesozoic cover [39], isolated blocks derived from intrabasinal provenance [34], or fragments of sedimentary successions dismembered by deformation processes [40]. The complex PKB structure results from at least four tectonic stages deforming strata derived from the eastern Piemont–Ligurian Ocean (Vahic Ocean) [41–44]. During Late Cretaceous, north verging thrust folding caused the transformation of PKB sedimentary sequences into individual tectonic units. At the Cretaceous–Palaeocene boundary, a marginal part of the southernmost Outer Carpathian basin system became tectonically part of PKB as the Grajcarek Unit. During Early Miocene (Savian phase), the strike-slip movements and development of the megabreccia and mega-boudinage resulted in the horst structure of the PKB. During the Middle Miocene, subsequent folding, regional compression, and progress and reactivation of transverse strike slip-faults cut PKB along the NNW–SSE direction, sub-parallel to the Tesisyre–Tornquist Zone (TTZ) [45,46].

PKB represents a sub-vertical 20 km wide and 600 km long strike-slip zone resulting from transpression between the North European Platform and the Central Western Carpathians, separating the Central and Outer Carpathian units. Units of the Central Carpathians correspond to the eastern Alps. Both presently form the ALCAPA system, interpreted to result from Oligocene to Middle Miocene lateral extrusion of fragments of Alpine–Carpathian units away from the convergence zone between the Adria and Eurasia continents (e.g., [46–49]). PKB tectonic structure alteration is due to the variations within the underplated North European Platform cut by several deep fracture zones parallel to the TTZ. The most important feature of these fracture zones is the prolongation of the boundary of Upper Silesian and Małopolska blocks (Kraków–Myszków Fault Zone) below the Carpathians [50]. Surface evidence of this zone in the PKB follows the Dunajec Fault, and the andesite dykes which have an en echelon relationship to this fault [28]. Along this deep fracture zone, the platform basement in its eastern side is downthrown in a stair-step fashion by approximately 3 km compared to the western side of this fault [51].

The Grajcarek Unit is the most external part of the Pieniny Klippen Belt in Poland, and it is considered a transitional zone between the Outer and Central Carpathian domains [56–59] (Figure 1b). The Grajcarek sedimentary succession represents strongly deformed slices consisting of Jurassic–Cretaceous siliciclastic and carbonate deposits overlain by Upper Cretaceous–Palaeocene sedimentary breccia, and numerous Triassic–Early Cretaceous carbonate/siliceous olistoliths formed in the southernmost margin of the Outer Carpathian realm and incorporated to PKB during the Laramian phase [27,29,57]. The thickness of the Grajcarek Succession, ranging from 400 to 900 metres, is mostly composed of siliciclastic rocks but also includes carbonate rocks that can be as much as 30–50 m thick (Figure 2). The Grajcarek Succession, belonging to the Northern Tethys realm, was deposited in an oceanic trough that opened in the southernmost Outer Carpathian domain as a result of the Triassic platform break-up during the North European plate rifting [54]. The Outer Carpathian basinal system was separated from the Pieniny Klippen basin (the northern part of the Inner Carpathian domain) by the mid-oceanic Czorsztyn Ridge to the south which emerged during the Bajocian [39]. The Grajcarek Succession was deposited on the north slope of the Czorsztyn Ridge. The sequence starts from deep water “black flysch”

of the Szlachtowa Formation. The age of the Szlachtowa Formation is still undetermined in spite of numerous studies based on the stratigraphy of various micro- and macrofacies, supporting both the Jurassic (Toarcian to ?Bajocian) (e.g., [55,60]) and Cretaceous ages (Albian–Cenomanian) (e.g., [61,62]).

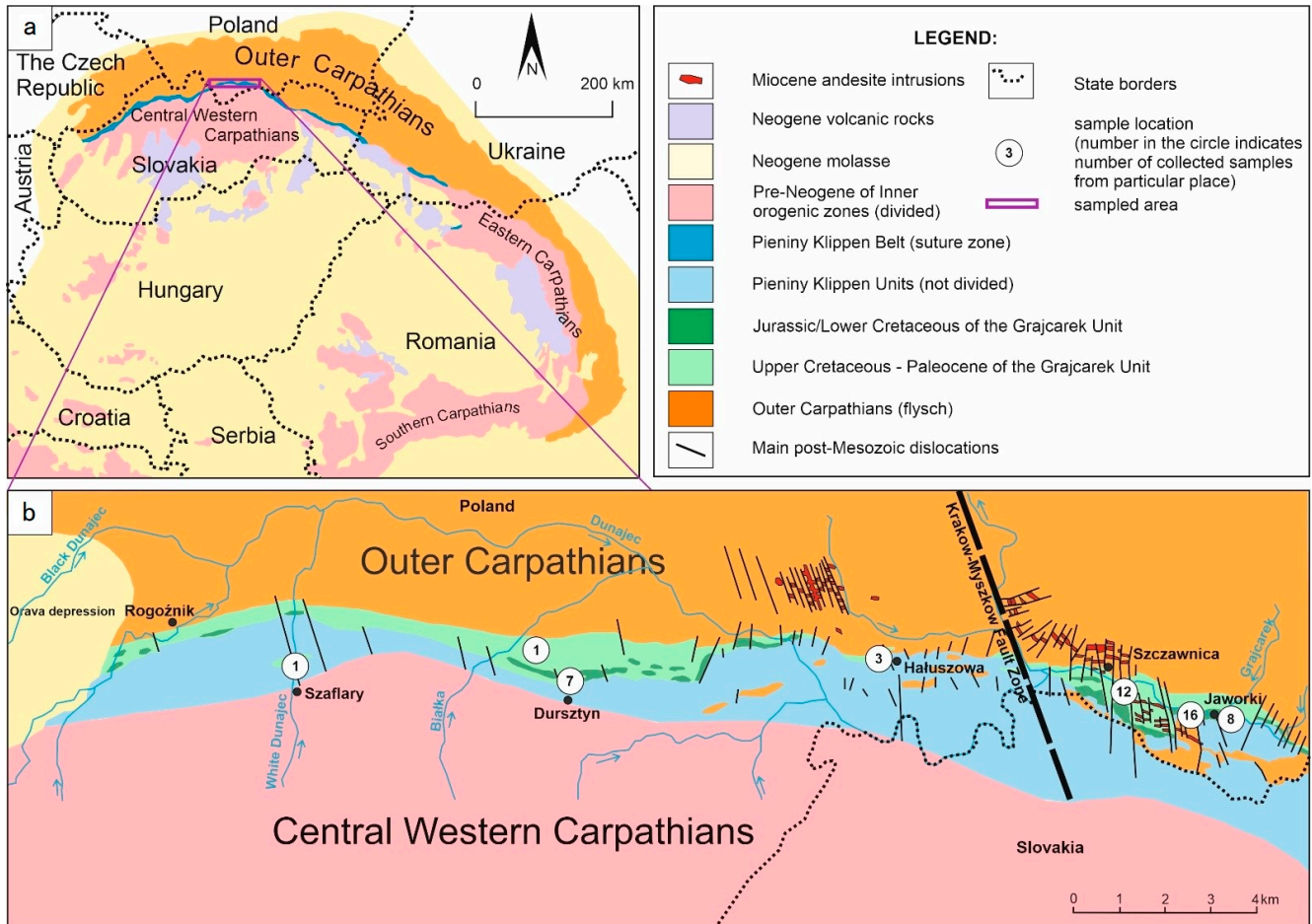


Figure 1. (a) Geological map of the Carpathians and adjacent areas with the location of investigated area (modified from [52–54]); (b) enlarged sample area marked in (a) showing the simplified geological structure of the Pieniny Klippen Belt of Poland (modified from [55]).

The shaly dominated Szlachtowa Formation is followed by the dysoxic sedimentation of the Opaleniec Formation in the Bajocian–Bathonian. Subsequently, the Sokolica and Czajakowa (Callovian–Oxfordian) formations represent wide-spread deposition of abyssal radiolarites and shales that are overlain by red nodular limestones of the Czorsztyn Limestone Formation (Kimmeridian–Lower Tithonian) and a thick package of pelagic cherty carbonates of the Pieniny Limestone Formations (Tithonian–Aptian). The upper section of the Lower Cretaceous is characterized by pelagic shales and marls of the Kapuśnica, Wronine, and Hulina formations that are overlain by red shales of the Malinowa Shale Formation that pass towards the top to grey flysch-like deposits of the Hałuszowa Formation. The Grajcarek Succession ends with the mixture of sedimentary breccias and proximal and distal flysch facies of the Maastrichtian–mid-Palaeocene Jarmuta Formation (e.g., [54]).

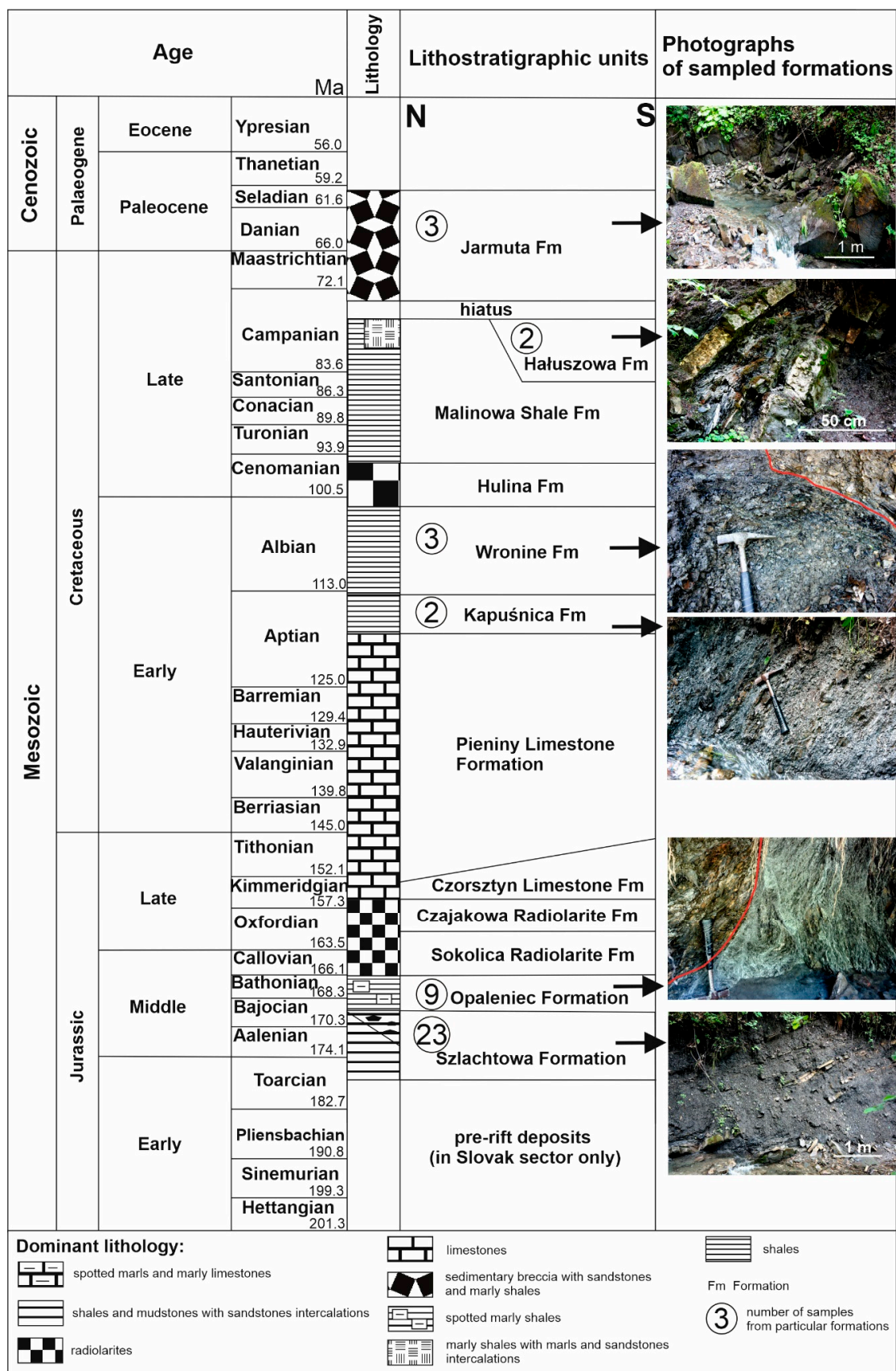


Figure 2. Lithostratigraphic scheme of the Grajcarek Succession in the Pieniny Klippen Belt (modified from [54]).

2. Materials and Methods

The paper describes 42 new organic petrographic and 39 vitrinite reflectance analyses from 42 samples representing the outcropping Grajcarek Succession, particularly Jurassic–Palaeocene siliciclastic rocks (23 samples from the Szlachtowa Formation; 9 samples from the Opaleniec Formation; 2 samples from the Kapuśnica; 3 samples from the Wronine Formation, and 3 from the Jarmuta Formation) (see Figure 2; Table A1). This paper assumed the Szlachtowa Formation both as Jurassic and the oldest deposits within the Grajcarek Succession.

Samples were collected from shales, marly shales, and mudstones representing the Grajcarek Succession (Figure 2; Table 1). Sampling site selection was imposed by regional distribution of shaly and marly facies rich in organic matter within the Grajcarek Succession, wherein the Szlachtowa Formation is the most-spread formation in the area study. There are only a few exposures of other sampled formations. Carbonates and the Malinowa Shale formations were excluded from sampling due to the lack of terrigenous particles. It should be also emphasized that the Grajcarek Unit occurs in the form of thin, strong deformed slices; hence, the state of natural exposures is variable and the thickness of particular formations is reduced.

The samples were prepared according to standardised procedures described in ISO 7404-5:2009 [63] and ASTM D7708-11 [64]. Samples were prepared as rock particles and then mounted in epoxy resin and polished. The random vitrinite reflectance measurements were done in reflected, non-polarised, monochromatic light ($\lambda = 546 \text{ nm}$) under oil immersion ($n = 1.518$) using a Zeiss Axioplan2 microscope. Maceral group identification proceeded in reflected white light and fluorescence following the procedures described in ISO 7404-3 (2009), under the ICCP (International Committee for Coal and Organic Petrology) requirements [65–67]. Petrographic classification of organic matter under the microscope discriminated diagenetic indigenous vitrinite from reworked detrital vitrinite, vitrinite-like macerals, and inertinite particles. Moreover, the presence or absence of fluorescent vitrinite macerals and VR suppression was noted during petrographic observations. The scatter in vitrinite reflectance data adds complexity and uncertainty to palaeotemperature calculation. In this paper, the effects of the depositional environment, diagenetic alterations, and pressure on the evolution of vitrinite reflectance in the Grajcarek Unit are discussed, noting that a lower random vitrinite reflectance caused by solid bitumen has previously been reported within the black shaly deposits in the Outer Carpathians [68,69].

Subsequently, the results of random vitrinite reflectance were the basis to calculate the T-peak (maximum burial temperature) using the linear equation $\ln(\text{VRr}) = 0.0124 \text{ T-peak} - 1.68$, established by [70] as a strong correlation between VR and T-peak. Maximum burial temperature and heating duration are commonly accepted as the principal controls for thermal maturation of sedimentary organic matter. Numerous studies prove that the effect of heating duration is limited, and after reaching maximum temperature, organic matter stabilises and discontinues significant reaction [71–76]. Therefore, VR, a well-established measure of thermal maturity, should be a function of T-peak reached during burial in the system [76–78].

The average standard deviation value of vitrinite reflectance in this paper was 0.14, and the resulting error for temperature estimation was $\pm 15 \text{ }^\circ\text{C}$. Subsequently, calculated T-peak data and geothermal gradient values taken from the literature were used to estimate burial depths of the sedimentary succession. Estimation of burial depths was carried out based on different values of the geothermal gradient as a consequence of its variability in PKB and adjacent areas. The geothermal gradient in the Maruszyna IG-1 and Hanusovce-1 deep boreholes located in the area of the PKB was 19.8 and 29.18 $^\circ\text{C}/\text{km}$, respectively. The lowest geothermal gradient was calculated based on fluid inclusion data from the southernmost part of the Outer Carpathian units, and it was 16.5 $^\circ\text{C}/\text{km}$ [79]. Nevertheless, such a low palaeogradient is quite typical for subduction-related accretionary complexes (e.g., [80]). Similar palaeogradient figures, as low as approximately 10 $^\circ\text{C}/\text{km}$, were calculated by Kotulová [81] based on vitrinite reflectance data from deep boreholes in

Eastern Slovakia. The calculated burial depths should be treated as relative data assuming that tectonic loading was the major burial mechanism and the main factor determining the organic matter thermal maturity.

The obtained data were used to develop a 2D contour map of regional thermal maturity distribution within the Grajcarek Succession using a kriging algorithm in the Surfer software package.

Table 1. Qualitative organic petrography results.

Sample	Formation	VR (%)	Maceral Group				Other OM Petrographic Features			
			Vitrinite	Vitrinite-Type	Inertinite	Liptinite	Pyritization	SB	OH	Oxidation
JJF1	Jarmuta	0.75	■	A, B	■	■	p	p	a	a
JJF2		0.83	■	A, B	■	■	p	a	a	a
JJF3		0.58	■	A, B	■	■	p	p	a	a
Hlsz1pw	Hałuszowa	0.83	■	A, B	■	■	p	a	a	a
Hlsz2		1.01	■	A	■	■	p	a	p	a
SzWr1	Wronine	n.d.*	■		■	■	a	a	a	p
SzWr2		0.88	■		■	■	a	a	a	p
SzWr		0.91	■	C	■	■	a	a	a	p
SzKap1	Kapuśnica	0.80	■	A	■	■	a	p	a	a
SzG1		0.76	■	A, B, C	■	■	a	p	a	a
SzOp1	Opaleniec	0.67	■	A, C	■	■	a	a	a	p
SzOp2		0.80	■	A	■	■	a	a	a	p
HIOp		n.d.*	■		■	■	a	a	a	p
DOp1		1.01	■	A, C	■	■	a	a	a	a
DOp2		0.89	■	A	■	■	a	a	a	p
DOp3		1.01	■	A, C	■	■	a	a	a	a
DSzl1		0.79	■	A, C	■	■	a	a	a	a
DSzl2		1.00	■	A, C	■	■	a	a	a	a
Krt1		n.d.*	■	A, C	■	■	a	a	a	a
1-12		Szlachtowa flysch to hemipelagic deposits	0.75	■	A, B	■	■	p	a	a
BW2a	0.87		■	A	■	■	p	p	p	a
BW2pb	0.61		■	A	■	■	p	p	a	a
JJF4	0.72		■	A, B, C	■	■	p	p	a	a
SzSzl1	0.78		■	A	■	■	p	p	a	a
SzSzl2	0.92		■	A	■	■	p	a	a	a
SzSzl3	0.90		■	A	■	■	p	p	a	a
SzSzl4	0.84		■	A, B	■	■	p	p	a	a
Jar1	0.81		■	A	■	■	p	p	p	a
SzlSzt1	0.78		■	A, B	■	■	p	p	p	a
SzlSzt2	0.82		■	A, B	■	■	p	p	p	a
SzlSzt3	0.79		■	A, B	■	■	p	p	a	a
SzlSzt4	0.69		■	A	■	■	p	p	a	a
SzlSzt5	0.75		■	A	■	■	p	p	a	a
SzlSzt6	0.79		■	A	■	■	p	a	a	a
SzlSzt7	0.97		■	A	■	■	p	p	a	a
SzlKr1	0.72		■	A	■	■	p	p	a	a
SzlKr2	0.85		■	A, B	■	■	p	p	a	a
SzlKr3	0.86		■	A, B	■	■	p	a	p	a
SzlKr4	0.76		■	A, B	■	■	p	p	p	a
SzlKr5	0.74		■	A	■	■	p	a	a	a
DSzl3	0.90		■	A	■	■	p	p	a	a
DSzl4	1.10		■	A	■	■	p	p	a	a

* Not determined; VR—vitrinite reflectance; vitrinite type A—indigenous, B—hydrogen-rich, and C—reworked. Other OM (organic matter) petrographic features: a—absent; OH—oil hydrocarbons; p—present; SB—solid bitumen. Maceral group: White—absence, grey—sporadic, dark grey—frequent.

3. Results

3.1. Organic Matter Petrography

Organic particles represent DOM (dispersed organic matter), a mixture of heterogeneous organic contents. Characteristics of this mixture depends on origin, type, and nature of organic matter (including marine, terrestrial, reworked) as well as early diagenesis and thermal maturity that follow the sediment burial (e.g., [82–84]). This point is essential, because some factors suppress vitrinite reflectance and cause difficulties in determining the proper thermal maturity of organic matter. The suppression of vitrinite reflectance in coal or dispersed organic matter could be caused by (a) perhydrous vitrinite or vitrinite-like macerals due to the lipid incorporation (caused by variations in pH conditions or the chemistry of various plant components) derived from lignin, cellulose, or tannin (e.g., [85–87]), (b) the impregnation of bitumen or incorporation of migrated oil (e.g., [87–89]), (c) the abundance of liptinite macerals in a vitrinite poor-source rock (e.g., [90–92]) or (d) variable bacterial activity in sediments [93].

Organic matter assemblages differ among the formations. The liptinite group predominates in the Szlachtowa Formation, and it is also frequent in the Jarmuta Formation (Table 1). In contrast to the flysch sediments, the liptinite macerals in hemipelagic deposits are sporadic or absent. Liptinites occur mainly as liptodetrinite (Figure 3a), sometimes impregnated by pyrite (Figure 3b). Macerals, such as alginite (telalginite), sporinite, cutinite, and suberinite, are also present (Figure 3). Alginite is a spongy or thin layered (flattened) structure, greenish yellow to orange, under oil immersion fluorescence (Figure 3b,c). Sporinite is usually compressed and aligned with bedding. It appears mainly as separate bodies and shows orange to brown under an oil immersion fluorescence (Figure 3d). Cutinite appears as bands with one edge, yellow to orange, under oil immersion fluorescence (Figure 3e). Suberinite represents cork tissue with empty cells (Figure 3e). In reflected white light, suberinite is from medium to dark grey, whereas it is brown in transmitted light. The liptinite macerals do not form clusters but are scattered in vitrinite macerals or in the mineral matrix.

The vitrinite group is present in all deposits, but the most abundant is in the Szlachtowa, Kapuśnica, and Jarmuta formations (Table 1). The vitrinite forms three varieties: indigenous vitrinite (type A), dark hydrogen-rich vitrinite (type B), and reworked/recycled vitrinite (type C). Type A represents angular to slightly rounded organic bodies with a homogenous structure including collotelinite and vitrodetrinite (Figure 3g,h). Collotelinite is characterised by a smooth surface and poorly preserved plant cell structure. In turn, vitrodetrinite forms sharp-edged fragments of vitrinite with a diameter of less than 20 µm. Type B is associated with hydrogen-rich lipoidal substances occurring as dark grey streaks in vitrinite particles. Consequently, type-B exhibits a lower reflectance and more intense fluorescence than type A. It generally resembles collodetrinite (Figure 3i,j). The type B vitrinite fluorescence colour ranges from red orange to red brown. Vitrinite must have become enriched in hydrogen in order to observe secondary fluorescence in type-B vitrinite at lower rank (0.60–0.80%), because fluorescence is related to hydrogen content. Type C includes detrital, well-rounded, sometimes heterogeneous vitrinite particles which may exhibit alteration rims related to oxidation (Figure 3k), and it shows a higher reflectance than the type A and B.

The inertinite group consists mainly of inertodetrinite (Figure 3l), with a small amount of semifusinite, fusinite, and macrinite. Semifusinite and fusinite are usually found isolated within the mineral matrix, and they are characterised by empty cell lumens or infilling of clay minerals, carbonates, or pyrite (Figure 3m–o).

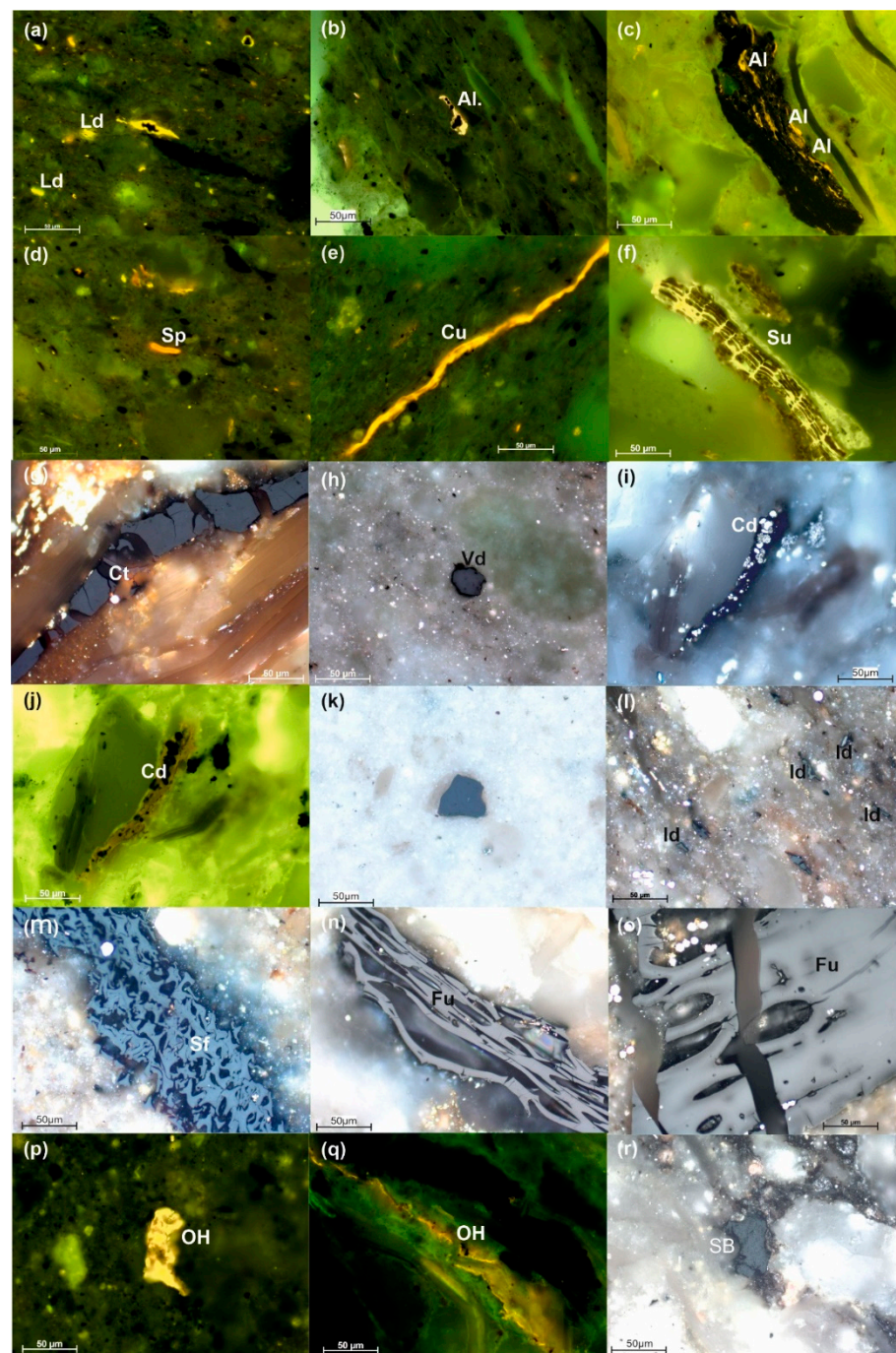


Figure 3. Microphotographs of organic matter: (a) typical liptodetrinite (Ld) particles in the Szlachtowa Fm, oil immersion, florescent light; (b) alginite in clay mineral matrix, Szlachtowa Fm-oil immersion; (c) flattened alginite (Al) in organic debris-Szlachtowa Fm, oil immersion, fluorescent light; (d) compressed sporinite (Sp) in clay minerals-Szlachtowa Fm, oil immersion, fluorescent light; (e) laminae of cutinite (Cu) parallel to the bedding plane in the Szlachtowa Fm, oil immersion, fluorescent light; (f) suberinite (Su) in the Kapuśnica Fm, oil immersion, reflected light; (g) collotelinite (Ct) laminae—Type A of vitrinite in the Szlachtowa Formation, oil immersion, reflected light; (h) well-rounded vitrodetrinite particle in the Szlachtowa Fm, oil immersion, reflected light; (i) collodetrinite (Cd) Type B of vitrinite impregnated by pyrite, the Szlachtowa Fm, oil immersion, reflected light; (j) the same photo as in (i), an example of collodetrinite (Cd) in oil immersion, fluorescent light; (k) sharp-edged vitrodetrinite (Vd) grain as Type C, the Jarmuta Fm, oil immersion, reflected light; (l) inertodetrinite (Id) scattered in the clay minerals, the Szlachtowa Fm, oil immersion,

reflected light; (m) empty cell lumens in semifusinite (Sf), the Szlachtowa Fm, oil immersion, reflected light; (n) arched and flattened fusinite (Fu), the Szlachtowa Fm, oil immersion, reflected light; (o) large particle of fusinite (Fu), oil immersion, reflected light; (p,q) liquid hydrocarbons (OHs) penetrating fractured mudstone of the Szlachtowa Fm, oil immersion, fluorescent light; (r) example of granular solid bitumen (SB) occupying the pore space in shaly matrix, the Szlachtowa Fm, oil immersion, reflected light.

Although the described maceral groups can be found in DOM, other structured components, specific to sedimentary rocks, are secondary products. These are liquid hydrocarbons and solid bitumen occurring mainly in the Szlachtowa Formation (Table 1). Liquid hydrocarbons appear as weathered films and exudates, rarely as drops, often penetrating pore spaces, fractures and calcite veins (Figure 3p,q). Granular solid bitumen occurs as non-fluorescence amorphous organic matter occupying larger intergranular pore spaces (Figure 3r). Pyritization and oxidation evidence in the organic matter (Table 1) are a consequence of the depositional environment, and they are essential pathways in determining suitable organic particles for VR measurements. The presence of pyrite in inclusions in organic particles was one of the seven criteria used by Benedict et al. [94] to discriminate indigenous vitrinite from oxidised/recycled vitrinite particles in American coals.

According to Murchison et al. [95], it is clear that the reflectance evolution path of recycled organic particles is located between vitrinite and inertinite groups or, more precisely, between hydrogen-rich and hydrogen-poor collotelinite and inertinite, respectively. During recycling, exposure to oxidation for variable durations progressively changes vitrinite into inertinite-like macerals that do not obey the same kinetic laws as indigenous vitrinite. The initial reflectance of these recycled materials reflects previous burial history and, consequently, cannot be used for thermal maturity assessment of their new host formation [96].

Organic petrography of the shaly deposits determined mixed type II/III (planktonic/humic) kerogen in the Szlachtowa, Kapuśnica, Hałuszowa, and Jarmuta formations and type III (terrestrial) in the Opaleniec Fm.

3.2. Thermal Maturity

Thermal maturity expressed by VR is variable through the whole Grajcarek Succession (Figure 4a; Table A1). Starting from the oldest strata, the Szlachtowa Formation, VR ranges from 0.65 to 1.10%. The Opaleniec Formation reveals similar VR values, from 0.67 to 1.01%. VR values in hemipelagic deposits represented by the Kapuśnica and Wronine formations ranging from 0.76 to 0.80% and from 0.88 to 0.91%, respectively. In turn, the thermal maturity of the youngest flysch formations (Hałuszowa and Jarmuta) is characterised by VR data from 0.83 to 1.10% and 0.58–0.83%, respectively. In general, the distribution of VR values shows that most samples are scattered from 0.70 to 0.90% (27 data points) and have a distinct geographical distribution. Smaller groups are in the range from 0.90 to 1.10% (8 data points) and from 0.50 to 0.70% (4 data points) (Figure 4b). VR values revealed thermally altered organic matter in the oil generation phase of so-called “oil window” (Figure 4a).

Regional thermal maturity distribution shows that the highest VR values are in the middle western part of the area, while a decrease in VR values was noted towards the east (Figure 5). A variation coefficient analysis (CV) showed low variability (less than 25%) in most samples. However, there was most remarkable CV diversity in the eastern part of the region. Ranges in VR data determined the maximum, calculated burial temperatures (T-peak) for particular formations (Table A1). The lowest (90–110 °C) and the highest (130–145 °C) T-peaks were calculated for the poor distributions. The main distribution displays temperatures in the range of 110–130 °C (Figure 4a).

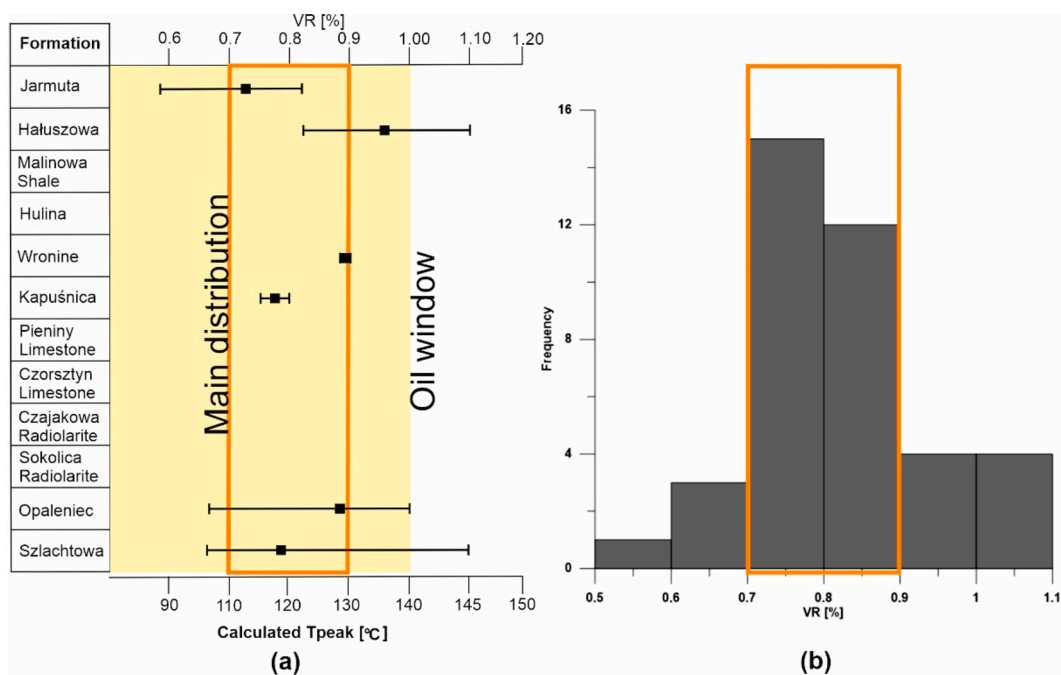


Figure 4. Thermal maturity analysis of the Grajcarek Succession: (a) VR ranges in particular formation with Calculated T-peak distributions; black squares indicate the average value in particular VR ranges; the yellow area shows a mature phase of oil generation. (b) Histogram of VR distribution among all data; the orange rectangle underlines VR main distribution.

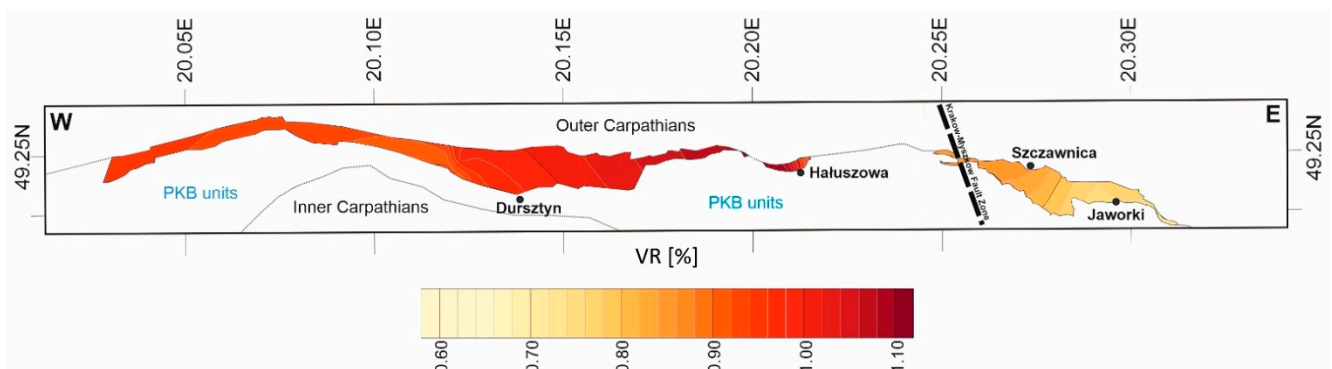


Figure 5. Regional thermal maturity distribution within the Grajcarek Jurassic–Palaeocene succession expressed by VR data.

3.3. Burial Depth

The depth of burial can be estimated from the maximum temperature and the geothermal gradient. Present-day data from boreholes indicate variations in thermal gradient in the Pieniny Klippen Belt, which suggests that paleothermal gradients might well have been variable in the past, too. Vitrinite reflectance values between 0.58–1.10% correspond to temperatures between 90 and 145 °C (± 15 °C) [71–75,97] with the duration of heating assumed to last until the post-depositional exhumation/uplift and cooling ages ranging between 32 and 12 Ma (e.g., [98]). In order to narrow the spread of the burial depth estimation, only data from the main VR measurement distribution (i.e., 0.70–0.90%) were calculated. Diverse geothermal gradients assumed in this paper resulted in a range of burial depths for T-peak values. For geothermal gradients of 16.5, 19.8, and 29.18 °C/km, burial depths displayed ranges from 5.5 to 8.7, 4.6–7.2, and 3.1–4.9 km, respectively. These estimated values are a measure of the maximum thicknesses of cover rock eroded.

4. Discussion

4.1. How Do Organic Matter Components Suppress Vitrinite Reflectance?

Apart from temperature, duration of heating, and pressure as the key factors affecting vitrinite reflectance during the coalification process, some factors can suppress or retard vitrinite reflectance data and cause difficulties in determining the proper thermal maturity of organic matter. VR evolution can be influenced by depositional and diagenetic effects such as enrichment in liptinite, sorption of products (bitumen) generated from lipoidal substance during maturation, and diagenetic formation of perhydrous vitrinite. These factors can result in data scatter in reflectance depth profiles and present challenges for interpretation of a paleogeothermal regime and organic matter maturity [86,99].

The presence of hydrogen-rich vitrinite, secondary products, and enrichment in liptinite could indicate VR suppression in the Grajcarek Unit, especially in the Szlachtowa Fm at lower VR distributions (~0.60–0.80%) (Table 1; Figure 4a). Under blue light excitation, a perhydrous type of vitrinite is evident as a brown-fluorescing organic particle observed in co-occurring liptinite enrichment. Huton et al. [100] noticed a considerable VR suppression in oil shales between samples lacking alginite and with 100% alginite content. Similar observations were recorded by Kalkreuth [101] in coal beds in British Columbia. He observed that higher concentrations of liptinite macerals resulted in a decrease in VR. Based on burial temperature, thermally mature, liptinite-rich Upper Miocene Modelo Formation source rock showed much lower VR than expected [102]. However, Newman and Newman [103] concluded that VR suppression was not influenced by high liptinite content. It was thought that vitrinite properties are strongly influenced by paleoenvironmental factors which control biochemical coalification (peat formation). According to the same authors, redox conditions in a depositional environment control vitrinite evolution, i.e., vitrinite exposed to anoxic conditions during early diagenesis in the marine environment is hydrogen-rich (perhydrous) and shows suppressed VR compared to vitrinite deposited under favourable aerobic conditions.

The frequently observed association with liptinite has led to an assumption that hydrogen-rich fluids (e.g., bitumen) are generated by biodegradation of liptinite and then absorbed into the vitrinite structure causing suppression of reflectance [89]. Although bitumen impregnation is commonly assumed to contribute to VR suppression, extraction of bitumen from source rock and coal samples determined by Barker et al. [104] showed an average 0.014% decrease in VR and, therefore, bitumen has a minor influence on suppressing VR.

On the other hand, Hackley et al. [88], during hydrous pyrolysis experiments on shale and coal samples, compared a maturation of vitrinite and associated solid bitumen. According to the authors, solid physical state and texture of solid bitumen are commonly identified under the microscope. However, solid bitumen can be misidentified as vitrinite when its optical features are not typical, which may explain some incorrect interpretations of VR measurements [88]. The problem of suppression is mentioned in this paper due to the different random vitrinite reflectances on various vitrinite particles in some samples (collected from the same formation) during the organic petrography analysis. A good example is represented by samples assigned as SzlSzt1 to SzlSzt7 (seven samples) from the Szlachtowa Formation collected from the same location. The VR values ranged from 0.67 to 0.97%. Assuming the elimination of measurement errors with an average standard deviation at the level of 0.14, the difference was visible in the results. Co-occurrence of hydrogen-rich vitrinite (type-B, so-called dark vitrinite) and liptinite maceral in one sample is the reason of this variance. Although the samples also contain type A vitrinite (indigenous vitrinite being the basis for VR measurements) often observed alongside the type B vitrinite; it could not be excluded that its “invisible” impregnation by a lipoidal substance was limited by microscope magnification. The distinction of indigenous from hydrogen-rich vitrinite has been conducted by differences in colour and fluorescence intensity. In this research, VR suppression was the reason for VR variability among samples representing the same formation which were collected from the same locality

(one measured section). Secondary vitrinite fluorescence is characteristic of syn- or post-depositional hydrogen enrichment and suppression as a record of depositional condition fluctuations (e.g., [99]).

The facies distribution within the Grajcarek Unit is not uniform. The facies differentiation emphasizes changes in short- and long-distance transport of clastic sediments (submarine slumps, turbidites, hemipelagic deposits) and various sources for organic matter. The latter is underlined by different maceral compositions in each formation, especially in the Szlachtowa Formation (Table 1). Mutual petrographic relations between hemipelagic and flysch formations are of high importance in assessing the thermal history reconstruction of sedimentary basins and structural evolution of the Grajcarek Unit during the Mesozoic. The Szlachtowa Formation was developed mainly as dark grey to black, fine to medium grained micaceous turbidites with intercalations of conglomeratic sandstones and crinoidal limestones. The turbidite facies are often replaced by the black shale facies. The Szlachtowa Formation deposition was dominated by extensional tectonics responsible for the graben–horst formation and resulting morphological troughs activity. The latter was dominated by hemipelagic sedimentation of black shales (e.g., [21]). The active rifting phase typically causes profound changes in factors controlling organic matter (OM) production and preservation (e.g., [105]).

4.2. Regional Thermal Maturity Distribution

VR values point to the low-grade alterations of the Grajcarek Unit with T-peaks ranging from 90 to 145 °C associated with maximum tectonic burial controlled by transpressional deformation, reached before exhumation and cooling. Low thermochronometric data from the PKB scattered widely, ranging from approximately 36 to 16 Ma [98] to 15–10 Ma [106], indicating that exhumation of the PKB occurred in Oligocene or Middle–Late Miocene. Thermal modelling by Botor et al. [107] indicated rapid tectonic burial and heating of freshly deposited sediments at approximately 30–28 Ma, whilst exhumation and cooling occurred immediately afterwards, approximately 28–25 Ma ago. AFT (apatite fission track) data from Jurassic sedimentary rocks in the PKB revealed ages ranging from 36 to 16 Ma which is in line with the stacking succession of the Outer Carpathian accretionary prism [98]. The various cooling ages might be related to sequential stacking of thrust imbricates and duplexes, accompanied by exhumation and erosion in a rear of the developing accretionary wedge with the maximum thickness of 20 km in the Pieniny area. The younger cooling ages (15–10 My) from the PKB are consistent with those of the surrounding Outer Carpathian units, thus confirming that the PKB formed as part of the fold-thrust-belt and did not experience a different thermal evolution [108]. The temperatures estimated from VR measurements in the northern vicinity of the PKB–Magura unit (Outer Carpathian domain) ranged from 110 to 125 °C [109], and they fell in the main Grajcarek temperature distribution. Thermal alteration of the selected samples from the Grajcarek Unit based on I/S ratio (smectite to illite transformation) indicated values ranging 100–135 °C, the same as or higher than those from the Magura Unit, close to the PKB [79]. Within the regional Grajcarek Unit distribution, there was a clear decrease in thermal alteration from west to east. The general pattern of palaeothermal gradients documented in accretionary wedges was low (e.g., [110]). Therefore, the lower geothermal gradient in the PKB (19.8 °C/km) was used in this discussion. The thickness of cover rock eroded in the area range between 4.6 and 7.2 km. The amount of erosion is greatest in the western part of the area which overlies the longitudinal deep fracture zone in the basement, being the southern prolongation of the Kraków–Myszków fault zone [29]. The contact between the Outer Carpathian and PKB domains was interpreted as a reverse fault thrusting the Pieniny Succession over the southernmost Outer Carpathian unit–Magura unit. During the Middle Miocene, that reverse fault was steepened by footwall imbrication and strike-slip deformation in the Late Miocene. Both tectonic periods resulted from the continental collision of the ALCAPA and Tisza–Dacia microplates with the European Plate occurring in the Middle–Late Miocene [111–113]. The underplated European Platform

basement with dextral deep fracture zones had a crucial role in the style of deformation resulting in the klippen structure of the PKB [29]. One of these zones, the Kraków–Myszków fault zone (Figures 1B and 5) (parallel to the TTZ) produced the displacement, which cut the PKB transversally into hanging (to the west) and footwall (to the east) segments with the down-going plate. Regional thermal differences within the Grajcarek Unit might regard this cumulative displacement around the Kraków–Myszków fault zone. The estimated T-peak of the footwall and hanging wall areas are 90–120 and 120–145 °C ± 15 °C, respectively. The area of the highest thermal alteration and greatest erosion in the adjacent fault zone here have been reported previously in the Rocky Mountains [114], South Wales Coalfield [115], the Appalachian Mountains [116], and in the Taiwan fold-thrust belts [117]. In cases where thrusting post-dates thermal maturation, sedimentary rocks that experienced higher-grade metamorphism are observed in a hanging wall [116].

Funding: This research was funded by a grant from the National Science Centre in Poland, No. 2019/03/X/ST10/00336.

Data Availability Statement: Data are included in figures, tables, and Appendix A; additional original data are available upon request from the author.

Acknowledgments: I thank the three anonymous reviewers whose comments and suggestions helped to improve and clarify this manuscript. I would like to thank Ewa Wójcik, who helped me collect samples and Magdalena Misz-Kennan for technical support. I would also like to thank Przemysław Gedl, who helped me to understand the complicated geology of the area studied.

Conflicts of Interest: The author declares no conflict of interest. The funders had no role in the study’s design, in the collection, analyses, or interpretation of data, in the writing of the manuscript, or in the decision to publish the results.

Appendix A

Table A1. Calculation of T-peak and burial depths for particular geothermal gradients values.

Sample Symbol	Formation	Age	VR (%)	SD	CV (%)	T-Peak (°C)	Estimated Burial Depth		
							19.8 °C/km	29.18 °C/km	16.5 °C/km
BW2a	Szlachtowa	J ₁ /J ₂	0.75	0.12	16.13	112	5.70	3.80	6.80
BW2pb	Szlachtowa	J ₁ /J ₂	0.87	0.22	25.63	124	6.30	4.30	7.70
JJF4	Szlachtowa	J ₁ /J ₂	0.61	0.12	19.18	96	4.80	3.30	5.80
JJF5	Szlachtowa	J ₁ /J ₂	0.72	0.27	38.33	109	5.50	3.70	6.60
SzSzl1	Szlachtowa	J ₁ /J ₂	0.78	0.14	17.94	115	5.80	4.00	7.00
SzSzl2	Szlachtowa	J ₁ /J ₂	0.92	0.13	13.91	121	6.50	4.40	7.80
SzSzl3	Szlachtowa	J ₁ /J ₂	0.90	0.12	13.89	127	6.40	4.30	7.70
SzSzl4	Szlachtowa	J ₁ /J ₂	0.84	0.14	17.02	121	6.10	4.20	7.30
Jar1	Szlachtowa	J ₁ /J ₂	0.81	0.13	16.29	133	6.70	4.50	8.10
SzLSzt1	Szlachtowa	J ₁ /J ₂	0.78	0.13	17.05	115	5.80	4.00	7.00
SzLSzt2	Szlachtowa	J ₁ /J ₂	0.82	0.15	18.29	119	6.00	4.10	7.20
SzLSzt3	Szlachtowa	J ₁ /J ₂	0.79	0.17	22.53	116	5.90	4.00	7.10
SzLSzt4	Szlachtowa	J ₁ /J ₂	0.69	0.14	20.58	105	5.30	3.60	6.40
SzLSzt5	Szlachtowa	J ₁ /J ₂	0.75	0.11	14.13	112	5.60	3.80	6.80
SzLSzt6	Szlachtowa	J ₁ /J ₂	0.79	0.18	23.54	116	5.90	4.05	7.10
SzLSzt7	Szlachtowa	J ₁ /J ₂	0.97	0.13	13.61	133	6.70	4.60	8.10
SzIKr1	Szlachtowa	J ₁ /J ₂	0.72	0.17	24.30	109	5.50	3.70	6.60
SzIKr2	Szlachtowa	J ₁ /J ₂	0.85	0.22	25.52	122	6.20	4.20	7.40
SzIKr3	Szlachtowa	J ₁ /J ₂	0.86	0.14	14.77	123	6.20	4.20	7.50
SzIKr4	Szlachtowa	J ₁ /J ₂	0.76	0.14	19.21	113	5.70	3.90	6.70
SzIKr5	Szlachtowa	J ₁ /J ₂	0.74	0.08	11.08	111	5.60	3.80	6.70
DSzl3	Szlachtowa	J ₁ /J ₂	0.90	0.15	17.11	127	6.40	4.30	7.70
DSzl4	Szlachtowa	J ₁ /J ₂	1.10	0.15	13.54	143	7.20	4.90	8.70
SzOp1	Opaleniec	J ₂	0.67	0.13	20.00	103	5.20	3.50	6.20

Table A1. Cont.

Sample Symbol	Formation	Age	VR (%)	SD	CV (%)	T-Peak (°C)	Estimated Burial Depth		
							19.8 °C/km	29.18 °C/km	16.5 °C/km
SzOp2	Opaleniec	J ₂	0.80	0.13	13.87	117	5.90	4.00	7.10
HlOp	Opaleniec	J ₂	n.d.*	n.d.	n.d.	n.d.	n.d.	n.d.	n.d.
DOP1	Opaleniec	J ₂	1.01	0.14	14.25	136	6.70	4.70	8.20
DOP2	Opaleniec	J ₂	0.89	0.18	20.33	126	6.40	4.30	7.60
DOP3	Opaleniec	J ₂	1.01	0.16	16.33	136	6.90	4.70	8.30
DSzl1	Opaleniec	J ₂	0.79	0.15	19.24	116	5.90	4.00	7.10
DSzl2	Opaleniec	J ₂	1.00	0.12	12.40	135	6.80	4.60	8.20
Krt1	Opaleniec	J ₂	n.d.	n.d.	n.d.	n.d.	n.d.	n.d.	n.d.
SzKap1	Kapuśnica	Cr ₁	0.80	0.15	19.5	117	5.90	4.00	7.10
SzG1	Kapuśnica	Cr ₁	0.76	0.13	17.63	113	5.70	3.90	6.90
SzWr1	Wronine	Cr ₁	n.d.	n.d.	n.d.	n.d.	n.d.	n.d.	n.d.
SzWr2	Wronine	Cr ₁	0.88	0.13	14.65	125	6.30	4.30	7.60
SzfWr	Wronine	Cr ₁	0.91	0.10	11.31	128	6.30	4.30	7.50
Hłsz1pw	Hałuszowa	Cr ₂	0.83	0.07	8.80	120	6.10	4.10	7.30
Hłsz2	Hałuszowa	Cr ₂	1.01	0.10	9.45	136	6.90	4.60	8.20
JJF1	Jarmuta	Cr ₂ /Pl	0.75	0.15	18.96	112	5.70	3.80	6.80
JJF2	Jarmuta	Cr ₂ /Pl	0.83	0.17	21.44	120	6.10	4.10	7.30
JJF3	Jarmuta	Cr ₂ /Pl	0.58	0.08	13.96	92	4.60	3.10	5.50

* Not determined; VR, Vitrinite reflectance; CV, coefficient of variation; J₁, Lower Jurassic; J₂, Middle Jurassic; Cr₁, Lower Cretaceous; Cr₂, Late Cretaceous; Pl, Palaeocene.

References

- Mukhopadhyay, P.K. Vitrinite reflectance as maturity parameter: Petrographic and molecular characterization and its applications to basin modeling. In *Vitrinite Reflectance as a Maturity Parameter: Applications and Limitations*; Mukhopadhyay, P.K., Dow, W.G., Eds.; American Chemical Society Symposium Series: Washington, DC, USA, 1994; Volume 570, pp. 1–24.
- Aderoju, T.; Bend, S.; Aderoju, T.; Bend, S. A comparative assessment of biomarker-based thermal maturity parameters. In *Petroleum Systems Analysis—Case Studies*; Abu Ali, M.A., Moretti, I.I., Nordgård Bolås, H.M., Eds.; AAPG Memoir: Tulsa, OK, USA, 2017; Volume 114, pp. 219–237.
- Abarghani, A.; Ostadhassan, M.; Bubach, M.B.; Zhao, P. Estimation of thermal maturity in the Bakken source rock from a combination of well logs, North Dakota, USA. *Mar. Petrol. Geol.* **2019**, *105*, 32–44. [[CrossRef](#)]
- Baig, I.; Faleide, J.I.; Jahren, J.; Mondol, N.H. Cenozoic exhumation on the southwestern Barents Shelf: Estimates and uncertainties constrained from compaction and thermal maturity analyses. *Mar. Petrol. Geol.* **2016**, *73*, 105–130. [[CrossRef](#)]
- Buchardt, B.; Lewan, M.D. Reflectance of vitrinite-like macerals as a thermal maturity index for Cambrian-Ordovician Alum Shale, southern Scandinavia. *AAPG Bull.* **1990**, *74*, 394–406.
- Bostick, N.H.; Pawlewicz, M.J. Paleotemperatures based on vitrinite reflectance of shales and limestones in igneous dike aureoles in the Upper Cretaceous Pierre Shale, Walsenburg, Colorado. In *Hydrocarbon Source Rocks of the Greater Rocky Mountain Region: Denver, CO; Rocky Mountain*; Woodward, J., Meissner, F.F., Clayton, J.L., Eds.; Rocky Mountain Association of Geologists: Denver, CO, USA, 1984; pp. 387–392.
- Corrado, S.; Aldega, L.; Di Leo, P.; Giampaolo, C.; Invernizzi, C.; Mazzoli, S.; Zattin, M. Thermal maturity of the axial zone of the southern Apennines fold-and-thrust belt (Italy) from multiple organic and inorganic indicators. *Terra Nova* **2005**, *17*, 56–65. [[CrossRef](#)]
- Dewing, K.; Obermajer, M. Lower Paleozoic thermal maturity and hydrocarbon potential of the Canadian Arctic Archipelago: Bulletin of Canadian. *Petrol. Geol.* **2009**, *57*, 141–166.
- Laughland, M.M.; Underwood, M.B. Vitrinite reflectance and estimates of paleotemperature within the Upper Shimanto Group, Muroto Peninsula, Shikoku, Japan. *Geol. Soc. Am. Spec. Pap.* **1993**, *273*, 25–43.
- Levine, J.R.; Davis, A. The relationship of coal optical fabrics to Alleghanian tectonic deformation in the central Appalachian fold-and-thrust belt, Pennsylvania. *Geol. Soc. Am. Bull.* **1984**, *101*, 1333–1337. [[CrossRef](#)]
- Miyakawa, A.; Kinoshita, M.; Hamada, Y. Thermal maturity structures in an accretionary wedge by a numerical simulation. *Prog. Earth. Planet Sci.* **2019**, *6*, 8. [[CrossRef](#)]
- Mori, K.; Taguchi, K. Examination of the low-grade metamorphism in the Shimanto Belt by vitrinite reflectance. *Mod. Geol.* **1988**, *12*, 325–339.
- O'Hara, K. Paleo-stress estimates on ancient seismogenic faults based on frictional heating of coal. *Geophys. Res. Lett.* **2004**, *31*, L03601.

14. Rusciadelli, G.; Viandante, M.G.; Calamita, F.; Cook, A.C. Burial-exhumation history of the central Apennines (Italy), from the foreland to the chain building: Thermochronological and geological data. *Terra Nova* **2005**, *17*, 560–572. [[CrossRef](#)]
15. Sakaguchi, A. High geothermal gradient with ridge subduction beneath Cretaceous Shimanto accretionary prism, southwest Japan. *Geology* **1996**, *24*, 795–798. [[CrossRef](#)]
16. Bullock, L.; Parnell, D.; Muirhead, D.; Armstrong, J.; Schito, A.; Corrado, S. A thermal maturity map based on vitrinite reflectance of British coals. *J. Geol. Soc.* **2019**, *176*, 1136. [[CrossRef](#)]
17. Corrado, S.; Invernizzi, C.; Mazzoli, S. Tectonic burial and exhumation in a foreland fold and thrust belt: The Monte Alpi case history (Southern Apennines, Italy). *Geodin. Acta* **2002**, *15*, 159–177. [[CrossRef](#)]
18. Pollastro, R.M.; Barker, C.E. Application of clay minerals, vitrinite reflectance and fluid inclusion studies to the thermal and burial history of the Pindale anticline, Green River basin, Wyoming. In *Roles of Organic Matter in Sediment Diagenesis*; Gautier, D.L., Ed.; SEPM Special Publications: Tulsa, OK, USA, 1986; Volume 38, pp. 73–83.
19. Nemčok, M.; Pospíšil, L.; Lexa, J.; Donelick, R.A. Tertiary subduction and slab break-off model of the Carpathian-Pannonia region. *Tectonophysics* **1998**, *295*, 307–340. [[CrossRef](#)]
20. Froitzheim, N.; Plašienka, D.; Schuster, R. Alpine tectonics of the Alps and Western Carpathians. In *The Geology of Central Europe; 2: Mesozoic and Cenozoic*; McCann, T.T., Ed.; Geological Society Publishing House: London, UK, 2008; pp. 1141–1232.
21. Birkenmajer, K. Preliminary revision of the stratigraphy of the Pieniny Klippen Belt series in Poland. *Bull. L'académie Pol. Sci. Cl.* **1953**, *3*, 271–274.
22. Ratschbacher, L.; Frisch, W.; Linzer, H.G.; Merle, O. Lateral extrusion in the Eastern Alps. Part 2: Structural analysis. *Tectonics* **1991**, *10*, 257–271. [[CrossRef](#)]
23. Ratschbacher, L.; Merle, O.; Davy, P.; Cobbold, P. Lateral extrusion in the eastern Alps. Part 1: Boundary conditions and experiments scaled for gravity. *Tectonics* **1991**, *10*, 245–256. [[CrossRef](#)]
24. Ratschbacher, L.; Frisch, W.; Linzer, H.G.; Sperner, B.; Meschede, M.; Decker, K. The Pieniny Klippen Belt in the Western Carpathians of northeastern Slovakia: Structural evidence for transpression. *Tectonophysics* **1993**, *226*, 471–483. [[CrossRef](#)]
25. Aubrecht, R.; Ožvoldová, L. Middle Jurassic-Lower Cretaceous development of the Pruské Unit in the western part of the Pieniny Klippen Belt. *Geol. Carpath.* **1994**, *45*, 211–223.
26. Nemčok, M.; Nemčok, J. Late Cretaceous deformation of the Pieniny Klippen Belt, West Carpathians. *Tectonophysics* **1994**, *239*, 286–294. [[CrossRef](#)]
27. Jurewicz, E. The contact between the Pieniny Klippen Belt and Magura Unit (the Małe Pieniny Mts.). *Geol. Quart.* **1997**, *41*, 315–326.
28. Jurewicz, E. Geodynamic evolution of the Tatra Mts. and the Pieniny Klippen Belt (Western Carpathians): Problems and comments. *Acta Geol. Polon.* **2005**, *55*, 295–338.
29. Jurewicz, E. The Šariš Transitional Zone, revealing interactions between Pieniny Klippen Belt, Outer Carpathians and European platform. *Swiss J. Geosci.* **2018**, *111*, 245–267. [[CrossRef](#)]
30. Birkenmajer, K.; Gedl, P.; Myczyński, R.; Tyszka, J. “Cretaceous black flysch” in the Pieniny Klippen Belt, West Carpathians: A case of geological misinterpretation. *Cretac. Res.* **2008**, *29*, 535–549. [[CrossRef](#)]
31. Schmid, S.M.; Bernoulli, D.; Fügenschyh, B.; Matenco, L.; Schefer, S.; Schuster, R.; Tischler, M.; Ustaszewski, K. The Alpine-Carpathian-Dinaridic orogenic system: Correlation and evolution of tectonic units. *Swiss J. Geosc.* **2008**, *101*, 139–183. [[CrossRef](#)]
32. Oszczytko, N.; Jurewicz, E.; Plašienka, D. Tectonics of the Klippen Belt and Magura Nappe in the eastern part of the Pieniny Mts. In *Western Carpathians, Poland and Slovakia—New approaches and results*. In Proceedings of the Congress of the Carpathian—Balkan Geological Association, Thessaloniki, Greece, 23–30 September 2010.
33. Barski, M.; Matyja, B.A.; Segit, T.; Wierzbowski, A. Early to Late Bajocian age of the so called “black flysch” (Szlachtowa Formation) deposits: Implications for the history and geological structure of the Pieniny Klippen Belt, Carpathians. *Geol. Quart.* **2012**, *56*, 391–410.
34. Plašienka, D. Jurassic syn-rift and Cretaceous syn-orogenic, coarse-grained deposits related to opening and closure of the Vahic (South Penninic) Ocean in the Western Carpathians—An overview. *Geol. Quart.* **2012**, *56*, 601–628. [[CrossRef](#)]
35. Plašienka, D.; Mikuš, M. Geological structure of the Pieniny and Šariš sections of the Klippen Belt between the Litmanová and Drienica villages in Eastern Slovakia. Bratislava. *Miner. Slovaca* **2010**, *42*, 155–178, (In Slovak, with English Summary).
36. Plašienka, D.; Soták, J. Evolution of Late Cretaceous-Palaeogene synorogenic basins in the Pieniny Klippen Belt and adjacent zones (Western Carpathians, Slovakia): Tectonic controls over a growing orogenic wedge. *Ann. Soc. Geol. Pol.* **2015**, *85*, 43–76. [[CrossRef](#)]
37. Plašienka, D.; Soták, J.; Aubrecht, R.; Michalík, J. Discussion of ‘Olistostromes of the Pieniny Klippen Belt Northern Carpathians. *Geol. Mag.* **2016**, *154*, 187–192. [[CrossRef](#)]
38. Krobicki, M.; Golonka, J. Geological history of the Pieniny Klippen Belt and Middle Jurassic Black Shales as one of the oldest deposits of this region—Stratigraphical position and palaeoenvironmental significance. *Geotourism* **2008**, *2*, 3–18. [[CrossRef](#)]
39. Golonka, J.; Krobicki, M.; Waśkowska, A.; Cieszkowski, M.; Ślącza, A. Olistostromes of the Pieniny Klippen Belt, Northern Carpathians. *Geol. Mag.* **2015**, *152*, 269–286. [[CrossRef](#)]
40. Plašienka, D. The Carpathian Klippen Belt and types of its klippen- an attempt at a genetic classification. *Miner. Slovaca* **2015**, *50*, 1–24.

41. Csontos, L.; Vörös, A. Mesozoic plate tectonic reconstruction of the Carpathian region. *Palaeogeogr. Palaeoclimatol. Palaeoecol.* **2016**, *210*, 1–56. [[CrossRef](#)]
42. Golonka, J.; Gahagan, L.; Krobicki, M.; Marko, F.; Oszczytko, N.; Ślącza, A. Plate tectonic evolution and paleogeography of the Circum-Carpathian Region. In *The Carpathians and Their Foreland: Geology and Hydrocarbon Resources*; Golonka, J., Picha, F., Eds.; AAPG Memoir: Tulsa, OK, USA, 2006; Volume 84, pp. 11–46.
43. Kováč, M.; Král, J.; Márton, E.; Plašienka, D.; Uher, P. Alpine uplift history of the Central Western Carpathians: Geochronological, paleomagnetic, sedimentary and structural data. *Geol. Carpath.* **1994**, *45*, 83–96.
44. Plašienka, D. Mesozoic evolution of Tatric units in the Malé Karpaty and Považský Inovec Mts.: Implications for the position of the Klappe and related units in western Slovakia. *Geol. Carpath.* **1995**, *46*, 101–112.
45. Plašienka, D. Dynamics of Mesozoic pre-orogenic rifting in the Western Carpathians. *Austrian J. Earth Sci.* **2003**, *94*, 79–98.
46. Krzywicz, P. Contrasting tectonic and sedimentary history of the central and eastern parts of the Polish Carpathian foredeep basin—results of seismic data interpretation. *Mar. Pet. Geol.* **2001**, *18*, 13–38. [[CrossRef](#)]
47. Csontos, L.; Nagymarosy, A.; Horváth, F.; Kováč, M. Tertiary evolution of the intracarpathian area: A model. *Tectonophysics* **1992**, *208*, 221–241. [[CrossRef](#)]
48. Csontos, L.; Nagymarosy, A. The Mid-Hungarian line: A zone of repeated tectonic inversion. *Tectonophysics* **1998**, *297*, 51–72. [[CrossRef](#)]
49. Haas, J.; Mioč, P.; Pamič, J.; Tomljenović, B.; Árkai, P.; Bérczi-Mak, A.; Koroknai, B.; Kovács, S.; Felgenhauer, E.R. Complex structural pattern of the Alpine–Dinaridic–Pannonian triple junction. *Int. J. Earth Sci.* **2000**, *89*, 377–389. [[CrossRef](#)]
50. Buła, Z.; Żaba, J. Structure of the Precambrian basement of the eastern part of the Upper Silesian block (Brunovistulicum). *Przegląd Geol.* **2008**, *56*, 473–480. (In Polish)
51. Zuchiewicz, W.; Oszczytko, N. Topography of the Magura floor thrust and morphotectonics of the Outer West Carpathians in Poland. *Ann. Soc. Geol. Pol.* **2008**, *78*, 135–148.
52. Kováč, M.; Nagymarosy, A.; Oszczytko, N.; Ślącza, A.; Csontos, L.; Marunteanu, M. Palinspastic reconstruction of the Carpathian-Pannonian region during the Miocene. In *Geodynamic Development of the Western Carpathians*; Raks, M., Ed.; Dionýz Štúr Publishers, Geological Survey of Slovak Republic: Bratislava, Czechoslovakia, 1998; pp. 180–217.
53. Golonka, J.; Pietsch, K.; Marzec, P. Deep structure of the Pieniny Klippen Belt in Poland. *Swiss J. Geosci.* **2019**, *112*, 475–506. [[CrossRef](#)]
54. Birkenmajer, K.; Gedl, P. The Grajcarek Succession (Lower Jurassic–Mid Paleocene) in the Pieniny Klippen Belt, West Carpathians, Poland: A stratigraphic synthesis. *Ann. Soc. Geol. Pol.* **2017**, *87*, 55–88. [[CrossRef](#)]
55. Gedl, P. Organic-walled dinoflagellate cyst stratigraphy of dark Middle Jurassic marine deposition of the Pieniny Klippen Belt, West Carpathians. *Stud. Geol. Pol.* **2008**, *131*, 7–227.
56. Plašienka, D. Continuity and Episodicity in the Early Alpine Tectonic Evolution of the Western Carpathians: How Large-Scale Processes Are Expressed by the Orogenic Architecture and Rock Record Data. *Tectonics* **2018**, *37*, 2020–2079. [[CrossRef](#)]
57. Jurewicz, E.; Segit, T. The tectonics and stratigraphy of the transitional zone between the Pieniny Klippen Belt and Magura Nappe (Szczawnica area, Poland). *Geol. Geoph. Environ.* **2018**, *44*, 127–144. [[CrossRef](#)]
58. Plašienka, D. Early stages of structural evolution of the Carpathian Klippen Belt (Slovakian Pieniny sector). *Miner. Slovaca* **2012**, *44*, 1–16.
59. Plašienka, D.; Józsa, Š.; Gedl, P.; Madzin, J. Fault contact of the Pieniny Klippen Belt with the Central Carpathian Paleogene Basin (Western Carpathians): New data from a unique temporary exposure in Ľutina village (Eastern Slovakia). *Geol. Carpath.* **2013**, *64*, 165–168. [[CrossRef](#)]
60. Birkenmajer, K.; Myczyński, R. Pilembachian (Early Jurassic) fauna from the Pieniny Klippen Belt, Carpathians, Poland: Its stratigraphic and palaeogeographic position. *Bul. Pol. Acad. Sci. Earth Sci.* **1994**, *42*, 223–245.
61. Golonka, J.; Rączkowski, W. *Explanations to the Detailed Geological Map of Poland, Sheet Piwniczna, 1:50,000*; Polish Geological Institute: Warszawa, Poland, 1984.
62. Oszczytko, N.; Malata, E.; Švábebenická, L.; Golonka, J.; Marko, F. Jurassic–Cretaceous controversies in the Western Carpathian flysch: The “black flysch” case study. *Cretaceous Res.* **2004**, *25*, 89–113. [[CrossRef](#)]
63. International Organization for Standardization. 7404-5:2009 (*Methods for the Petrographic Analysis of Coals—Part 5: Method of Determining the Reflectance of Vitrinite Microscopically*); International Organization for Standardization: Geneva, Switzerland, 2009.
64. American Society for Testing and Materials. ASTM D7708-11 (*Standard Test Method for Microscopical Determination of the Reflectance of Vitrinite Dispersed in Sedimentary Rocks*); American Society for Testing and Materials: West Conshohocken, PA, USA.
65. ICCP (International Committee for Coal and Organic Petrology). New vitrinite classification (ICCP system 1994). *Fuel* **1998**, *77*, 349–358. [[CrossRef](#)]
66. ICCP (International Committee for Coal and Organic Petrology). New inertinite classification (ICCP system 1994). *Fuel* **2001**, *80*, 459–471. [[CrossRef](#)]
67. Pickel, W.; Kus, J.; Flores, D.; Kalaitzidis, S.; Christanis, K.; Cardott, B.J.; Misz-Kennan, M.; Rodrigues, S.; Hentschel, A.; Hamor-Vido, M.; et al. Classification of liptinite—ICCP System 1994. *Int. J. Coal Geol.* **2017**, *169*, 40–61. [[CrossRef](#)]
68. Kotarba, M.J.; Więclaw, D.; Bilkiewicz, E.; Dziadzio, P.; Kowalski, A. Genetic correlation of source rocks and natural gas in the Polish Outer Carpathians and Paleozoic–Mesozoic basement east of Kraków (southern Poland). *Geol. Q.* **2017**, *61*, 569–589. [[CrossRef](#)]

69. Waliczek, M.; Machowski, G.; Więclaw, D.; Konon, A.; Wandycz, P. Properties of solid bitumen and other organic matter from Oligocene shales of the Fore-Magura Unit in Polish Outer Carpathians: Microscopic and geochemical approach. *Int. J. Coal Geol.* **2019**, *210*, 103206. [[CrossRef](#)]
70. Barker, C.E.; Pawlewicz, M.J. Calculation of vitrinite reflectance from thermal histories and peak temperatures, a comparison of methods. In *Vitrinite Reflectance as a Maturity Parameter: Applications and Limitations*; Mukhopadhyay, P.K., Dow, W.G., Eds.; American Chemical Society Symposium: Washington, DC, USA, 1994; Series 570; pp. 216–229.
71. Barker, C.E. The influence of time on metamorphism of sedimentary organic matter in selected geothermal systems, Western North America. *Geology* **1983**, *11*, 384–388. [[CrossRef](#)]
72. Barker, C.E. Temperature and time in the thermal maturation of sedimentary organic matter. In *Thermal History of Sedimentary Basins: Methods and Case Histories*; Neaser, N.D., McCulloh, T.H., Eds.; Springer: New York, NY, USA, 1989; pp. 73–98.
73. Barker, C.E. Implications for organic matter maturation studies of evidence for a geologically rapid increase and stabilization of vitrinite reflectance at peak temperature: Cerro Prieto Geothermal System, Mexico. *AAPG Bull.* **1991**, *75*, 1852–1863.
74. Burnham, A.K.; Sweeney, J.J. A chemical kinetic model of vitrinite maturation and reflectance. *Geochim. Cosmochim. Acta* **1989**, *53*, 2649–2657. [[CrossRef](#)]
75. Dow, W.G.; O'Connor, D.J. Kerogen maturity and type by reflected light microscopy applied to petroleum exploration. In *How to Assess Maturation and Palaeotemperatures*; Staplin, F.L., Ed.; SEMP Short Course No. 7; Society of Economic Paleontologists and Mineralogists: Tulsa, OK, USA, 1987; pp. 133–157.
76. Ercegovac, M.; Kostic, A.; Karg, H.; Welte, D.H.; Littke, R. Temperature and burial history modelling of the Drmno and Markovac depressions, SE Pannonian Basin, Serbia. *J. Petrol. Geol.* **2003**, *26*, 5–27. [[CrossRef](#)]
77. Huang, W.L. Experimental study of vitrinite maturation: Effects of temperature, time, pressure, water and hydrogen index. *Org. Geochem.* **1996**, *24*, 233–241. [[CrossRef](#)]
78. Waples, D.W. Thermal models for oil generation. In *Advances in Petroleum Geochemistry*; Brooks, J., Welte, D., Eds.; Academic Press: London, UK, 1984; pp. 7–67.
79. Świerczewska, A. The interplay of the thermal and structural histories of the Magura nappe (Outer Carpathians) in Poland and Slovakia. *Min. Polon.* **2005**, *36*, 91–144.
80. Peacock, S.M. Thermal and petrologic structure of subduction zones (overview). In *Subduction Top to Bottom*; Bebout, G.E., Scholl, D.W., Kirby, S.H., Platt, J.P., Eds.; American Geophysical Union: Washington, WA, USA, 1996; pp. 119–134.
81. Kotulová, J. Relation Analysis of Thermal Alteration of Flysch Sediments in the Eastern Slovakian Part of Western Carpathians. Ph.D. Thesis, Comenius University in Bratislava, Bratislava, Slovakia, 2010. (In Slovak with English Summary).
82. Florez, D.; Suárez-Ruiz, I. Organic Petrology in the Study of Dispersed Organic Matter. In *The Role of Organic Petrology in the Exploration of Conventional and Unconventional Hydrocarbon Systems*; Suárez-Ruiz, I., Filho, J.G.M., Eds.; Bentham Books: Sharjah, United Arab Emirates, 2017; Volume 43, pp. 37–46. [[CrossRef](#)]
83. Suárez-Ruiz, I.; Flores, D.; Filho, J.G.M.; Hackley, P.C. Review and update of organic petrology: Part 1, geological application. *Int. J. Coal Geol.* **2012**, *99*, 54–112. [[CrossRef](#)]
84. Costa, A.; Flores, D.; Suárez-Ruiz, I.; Pevida, C.; Rubiera, F.; Iglesias, M.J. The importance of thermal behavior and petrographic composition for understanding the characteristics of a Portuguese perhydrous Jurassic coal. *Int. J. Coal Geol.* **2010**, *84*, 237–247. [[CrossRef](#)]
85. Iglesias, M.J.; del Río, J.C.; Laggoun-Defarge, F.; Cuesta, M.J.; Suarez-Ruiz, I. Control of the chemical structure in perhydrous coals by FTIR and Py-GC/MS. *J. Anal. Appl. Pyrol.* **2002**, *62*, 1–34. [[CrossRef](#)]
86. Zhang, E.; Hatcher, P.G.; Davis, A. Chemical composition of pseudo-phlobaphinite precursors: Implications for the presence of aliphatic biopolymers in vitrinite from coal. *Org. Geochem.* **1993**, *20*, 721–734. [[CrossRef](#)]
87. Chen, Z.; Dewing, K.; Synnott, D.P.; Liu, X. Correcting Tmax suppression: A numerical model for removing adsorbed heavy oil and bitumen from Upper Ordovician source rocks, Arctic Canada. *Energy Fuels* **2019**, *33*, 6234–6246. [[CrossRef](#)]
88. Hackley, P.C.; Lewan, M. Understanding and distinguishing reflectance measurements of solid bitumen and vitrinite using hydrous pyrolysis: Implications to petroleum assessment. *AAPG Bull.* **2018**, *102*, 1119–1140. [[CrossRef](#)]
89. Peters, K.E.; Hackley, P.C.; Thomas, J.J.; Pomerantz, A.E. Suppression of vitrinite reflectance by bitumen generated from liptinite during hydrous pyrolysis of artificial source rock. *Org. Geochem.* **2018**, *125*, 220–228. [[CrossRef](#)]
90. Goodarzi, F.; Snowdon, L.; Gentzis, T.; Pearson, D. Petrological and chemical characteristics of liptinite-rich coals from Alberta, Canada. *Mar. Petrol. Geol.* **1994**, *11*, 307–319. [[CrossRef](#)]
91. Mastalerz, M.; Wilks, K.R.; Bustin, R.M. Variation in vitrinite chemistry as a function of associated liptinite content; a microprobe and FT-i.r. investigation. *Org. Geochem.* **1993**, *20*, 555–562. [[CrossRef](#)]
92. Petersen, H.I.; Vosgerau, H. Composition and organic maturity of Middle Jurassic coals, North-East Greenland: Evidence for liptinite-induced suppression of huminite reflectance. *Int. J. Coal Geol.* **1999**, *41*, 257–274. [[CrossRef](#)]
93. Quick, J.C. Iso-rank variation of vitrinite reflectance and fluorescence intensity. In *Vitrinite Reflectance as a Maturity Parameter: Applications and Limitations*; Mukhopadhyay, P.K., Dow, W.G., Eds.; American Chemical Society Symposium: Washington, WA, USA, 1994; Series 570; pp. 64–75.
94. Benedict, L.G.; Thompson, R.R.; Shigo, J.J.; Aikaman, R.P. Pseudovitrinite in Appalachian coking coals. *Fuel* **1968**, *47*, 125–143.
95. Murchison, D.G.; Cook, A.C.; Raymond, A.C. Optical properties of organic matter in relation to thermal gradients and structural deformation. *Philos. Trans. R. Soc. Lond.* **1985**, *315*, 157–486.

96. Nzoussi-Mbassani, P.; Copard, Y.; Disnar, J.R. Vitrinite recycling: Diagnostic criteria and reflectance changes during weathering and reburial. *Int. J. Coal Geol.* **2005**, *61*, 223–239. [[CrossRef](#)]
97. Khavari-Khorasani, G.; Michelsen, J.K. Thermal evolution of solid bitumens, bitumen reflectance and kinetic modelling of reflectance: Application in petroleum and ore prospecting. *Energy Sources* **1993**, *15*, 181–204. [[CrossRef](#)]
98. Anczkiewicz, A.A.; Świerczewska, A. Thermal history and exhumation of the Polish Western Outer Carpathians: Evidence from combined apatite fission track and illite-smectite data. In Proceedings of the 11th International Conference on Thermochronology, Anchorage, Alaska, 15–19 September 2008; pp. 1–4.
99. Kalinowski, A.A.; Gurba, L.W. Interpretation of vitrinite reflectance-depth profiles in the Northern Denison Trough, Bowen Basin, Australia. *Int. J. Coal. Geol.* **2020**, *219*, 103364. [[CrossRef](#)]
100. Hutton, A.C.; Cook, A.C. Influence of alginite on the reflectance of vitrinite from Joadja, N.S.W., and some other coals and oil shales containing alginite. *Fuel* **1980**, *59*, 711–714. [[CrossRef](#)]
101. Kalkreuth, W. Rank and petrographic composition of selected Jurassic-Lower Cretaceous coals of British Columbia, Canada. *Bull. Can. Pet. Geol.* **1982**, *30*, 112–139.
102. Walker, A.L.; McCulloch, T.H.; Petersen, N.F.; Stewert, R.J. Discrepancies between anomalously low reflectance of vitrinite and other maturation indicators from an Upper Miocene oil source rock, Los Angeles Basin, California. *AAPG Bull.* **1983**, *67*, 565.
103. Newman, J.; Newman, N.A. Reflectance anomalies in Pike River coals: Evidence of variability in vitrinite type, with implications for maturation studies and “Suggate rank”. *N. Z. J. Geol. Geophys.* **1982**, *25*, 233–243. [[CrossRef](#)]
104. Barker, C.E.; Lewan, M.D.; Pawlewicz, M.J. The influence of extractable organic matter on vitrinite reflectance suppression: A survey of kerogen and coal types. *Int. J. Coal Geol.* **2007**, *70*, 67–78. [[CrossRef](#)]
105. Rizzi, M.; Hovikoski, J.; Schovsbo, N.H.; Therkelsen, J.; Olivarius, M.; Nytoft, H.P.; Nga, L.H.; Thuy, N.T.T.; Toan, D.M.; Bojesen-Koefoed, J.; et al. Factors controlling accumulation of organic carbon in a rift-lake, Oligocene Vietnam. *Sci. Rep.* **2020**, *10*, 14976. [[CrossRef](#)] [[PubMed](#)]
106. Mazzoli, S.; Jankowski, L.; Szaniawski, R.; Zattin, M. Low-T thermochronometric evidence for post-thrusting (~11 Ma) exhumation in the Western Outer Carpathians, Poland. *CR Geosci.* **2010**, *342*, 162–169. [[CrossRef](#)]
107. Botor, D.; Dunkl, I.; Rauch-Włodarska, M.; von Eynatten, H. Attempt to dating of accretion in the West Carpathian Flysch Belt: Apatite fission track thermochronology of tuff layers. *Geolines* **2006**, *20*, 21–23.
108. Castelluccio, A.; Mazzoli, S.; Andreucci, B.; Jankowski, L.; Szaniawski, R.; Zattin, M. Building and exhumation of the Western Carpathians: New constraints from sequentially restored, balanced cross sections integrated with low-temperature thermochronometry. *Tectonics* **2016**, *35*, 2698–2733. [[CrossRef](#)]
109. Zielińska, M. Organic-matter vitrinite reflectance variability in the Outer Carpathians, Poland: Relationship to tectonic evolution. *Geol. Quart.* **2017**, *61*, 214–226. [[CrossRef](#)]
110. Sakaguchi, A. Thermal maturity in the Shimanto accretionary prism, southern Japan, with the thermal change with the subducting slab: Fluid inclusion and vitrinite reflectance study. *Earth Planet. Sci. Lett.* **1996**, *173*, 63–74.
111. Andreucci, B.; Castelluccio, A.; Jankowski, L.; Mazzoli, S.; Szaniawski, R.; Zattin, M. Burial and exhumation history of the Polish Outer Carpathians: Discriminating the role of thrusting and post-thrusting extension. *Tectonophysics* **2013**, *608*, 866–883. [[CrossRef](#)]
112. Săndulescu, M. Cenozoic tectonic history of the Carpathians, in The Pannonian Basin: A Study in Basin Evolution. *AAPG Mem.* **1988**, *35*, 17–25.
113. Matenco, L.; Bertotti, G.; Leever, K.; Cloetingh, S.; Schmid, M.; Tărăpoancă, M.; Dinu, C. Large scale deformations at a locked collisional boundary: Coeval Pliocene-Quaternary differential tectonic movements in the foreland of the SE Carpathians. *Tectonics* **2007**, *26*, TC4011. [[CrossRef](#)]
114. Bustin, R.M. Heating during thrust faulting in the Rocky Mountains: Friction of fiction? *Tectonophysics* **1983**, *95*, 309–328. [[CrossRef](#)]
115. Gayer, R.; Fowler, R.; Davies, G. Coal rank variations related to major thrust detachments in South Wales coalfield: Implication of fluid flow and mineralization. In *European Coal Geology and Technology*; Geological Society of London: London, UK, 1997; Volume 125, pp. 161–178.
116. O’Hara, K.; Hower, J.C.; Rimmer, S.M. Constraints on the emplacement and uplift history of the Pine Mountains thrust sheet, eastern Kentucky: Evidence from coal rank trends. *J. Geol.* **1990**, *98*, 43–51. [[CrossRef](#)]
117. Sakaguchi, A.; Yanagihara, A.; Ujiie, K.; Tanaka, H.; Kameyama, M. Thermal maturity of a fold-thrust belt based on vitrinite reflectance analysis in the Western Foothills complex, western Taiwan. *Tectonophysics* **2007**, *443*, 220–232. [[CrossRef](#)]